Supporting Information

Interface Synergistic Effect from Hierarchically Porous $Cu(OH)_2$@FCN MOF/CF Nanosheet Arrays Boosting Electrocatalytic Oxygen Evolution

Xue Li, Yinan Zheng, Hu Yao, Jiayu Bai, Siliang Yue and Xiaohui Guo *

Key Lab of Synthetic and Natural Functional Molecule Chemistry of Ministry of Education, College of Chemistry and Materials Science, Shaanxi Key Laboratory for Carbon Neutral Technology, Northwest University，Xi'an 710010, China; lxlxturbo@163.com (X.L.); zhengyinan1203@163.com (Y.Z.); 202020797@stumail.nwu.edu.cn (H.Y.); bjy2418785398@stumail.nwu.edu.cn (J.B.); yuesiliang98@163.com (S.Y.)

* Correspondence: guoxh2009@nwu.edu.cn

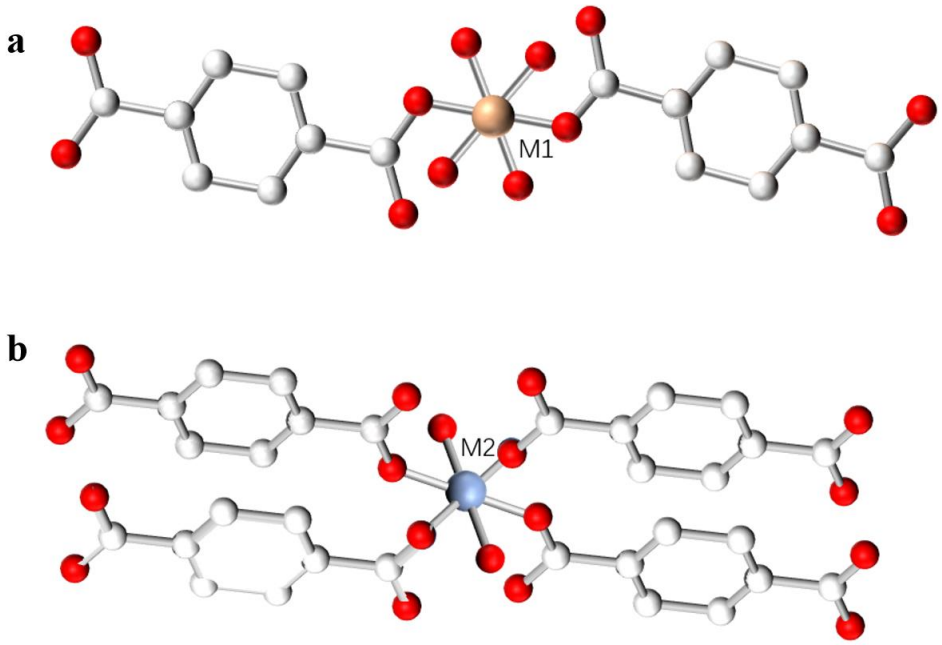
a
M1
b
M2
c
M1
M2
M2
M2
M2
M1
d
b
c
a
M1
M2

Figure S1. The two differently coordinated metal sites (a) M1 and (b) M2 metal ions are both octahedrally coordinated to six O atoms in MOF; (a) M1 metal ion is attached to four μ3-OH and two carboxylate oxygen atoms; (b) The M2 metal ion is linked to two μ3-OH and four carboxylate oxygen atoms; (c) Each BDC organic ligand is coordinated to six metal ions. These MO_6 (M = M1 or M2) octahedra are bridged along the c-axis by hydrogen-oxygen and further coordinated by hydrogen-oxygen and carboxylate oxygen atoms on the a- and b-axes to form the 3D MOF. Color codes: dark blue and yellow = metal, red = oxygen, silver-white = carbon.

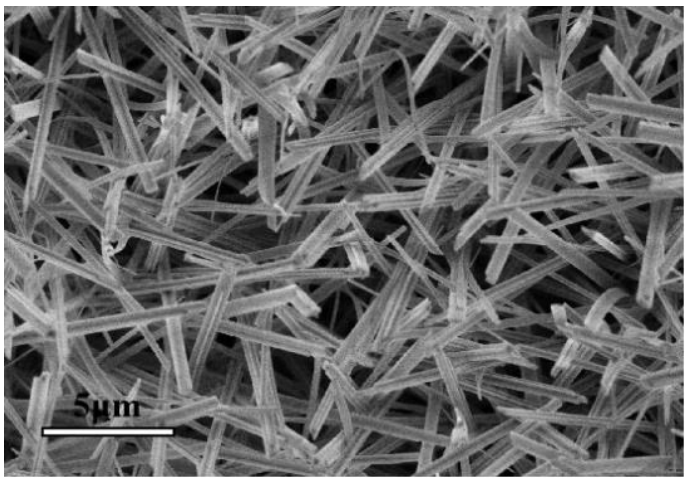

Figure S2. SEM image of $Cu(OH)_2$@CF.

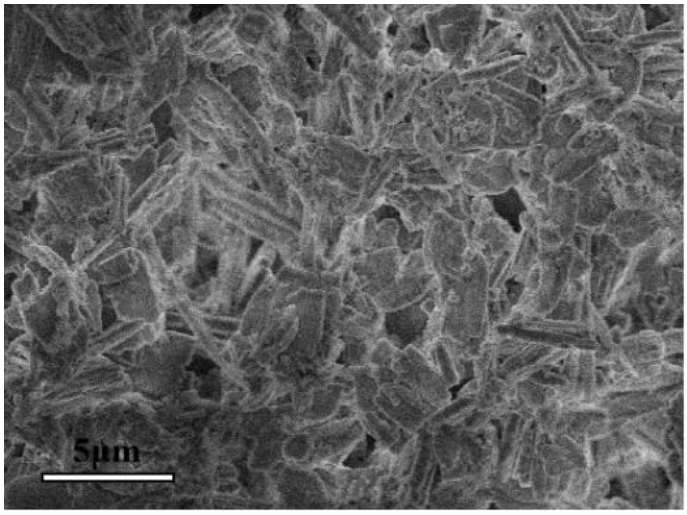

Figure S3. SEM image of FCN MOF/CF.

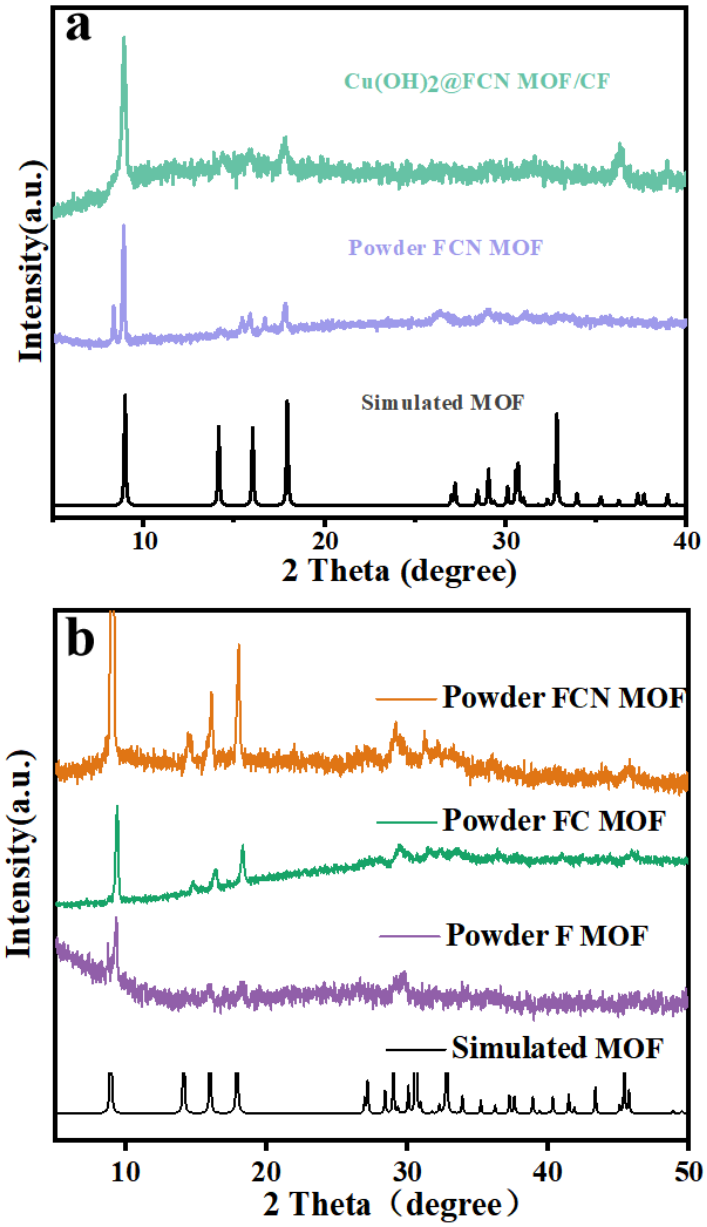

Figure S4. (**a**) Powder XRD patterns of $Cu(OH)_2$@FCN MOF/CF and Powder FCNMOF; (b) Powder XRD patterns of FCN-MOF, FC-MOF, F-MOF.

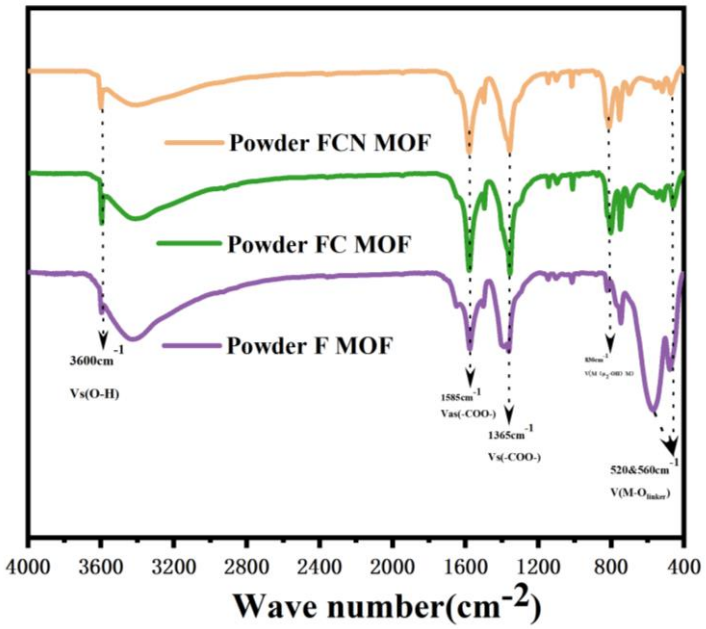

Figure S5. FT-IR spectra of FCN-MOF, FC-MOF, and F-MOF.

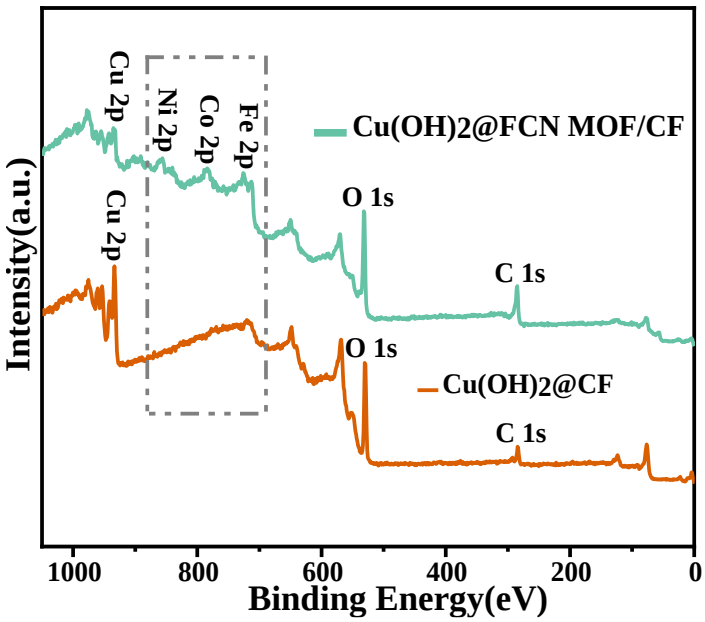

Figure S6. The survey XPS spectrum of our synthesized $Cu(OH)_2$@FCN MOF/CF and $Cu(OH)_2$@CF samples.

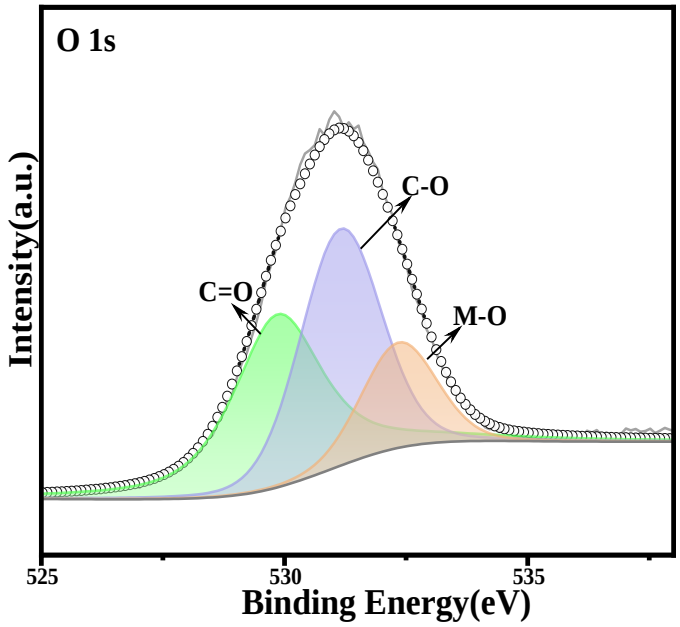

Figure S7. High-resolution XPS spectra of O1s of $Cu(OH)_2$@FCN MOF/CF.

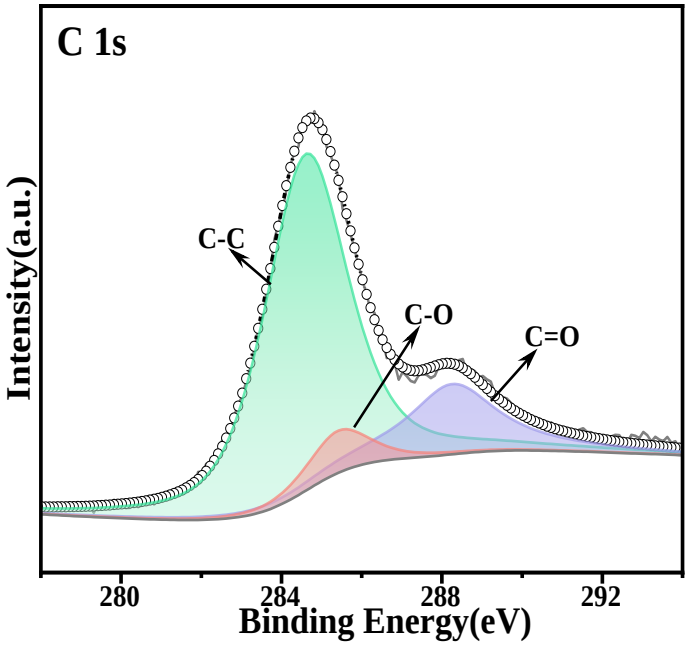

Figure S8. High-resolution XPS spectra of C1s of $Cu(OH)_2$@FCN MOF/CF.

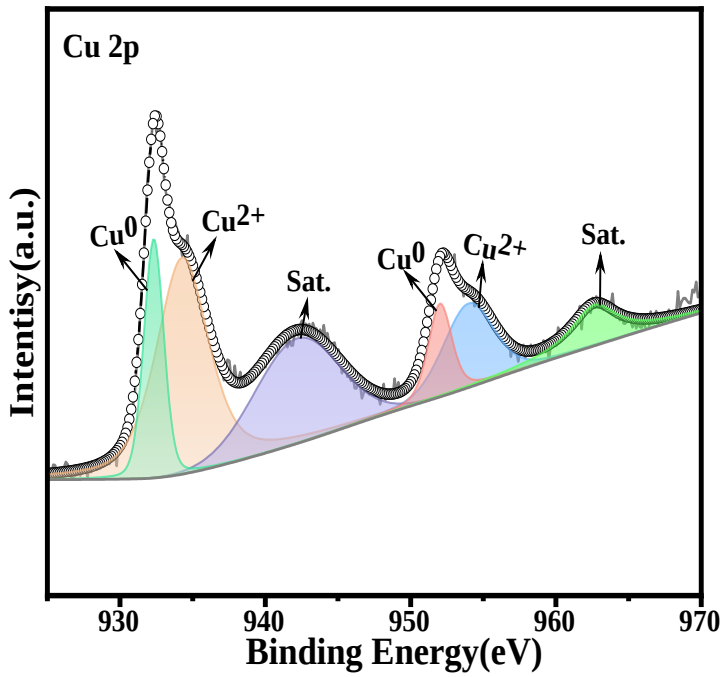

Figure S9. High-resolution XPS spectra of Cu 2p of $Cu(OH)_2$@FCN MOF/CF.

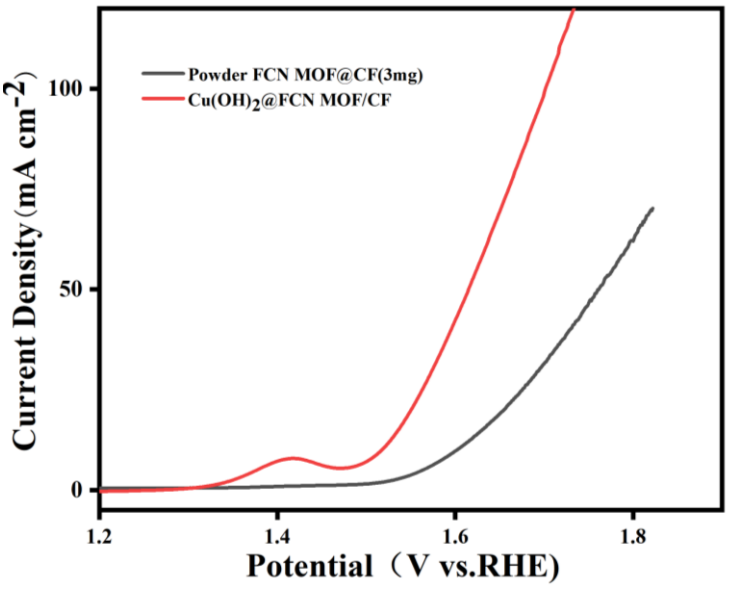

Figure S10. LSV curves of $Cu(OH)_2$@FCN MOF/CF and Powder FCN MOF@CF.

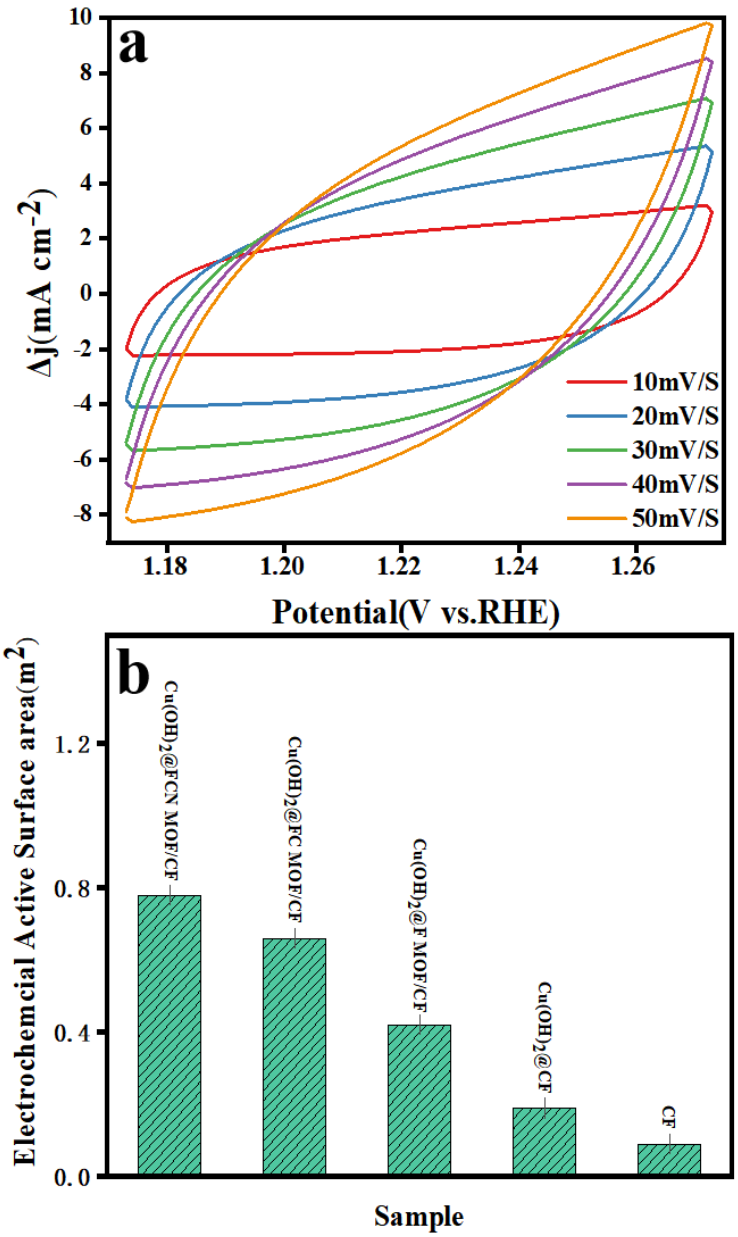

Figure S11. (**a**) CV curves of $Cu(OH)_2$@FCN MOF/CF at increasing scan rates (mV/S^{-1}); (b) ECSA values of $Cu(OH)_2$@MOF/CF catalysts with different metal species.

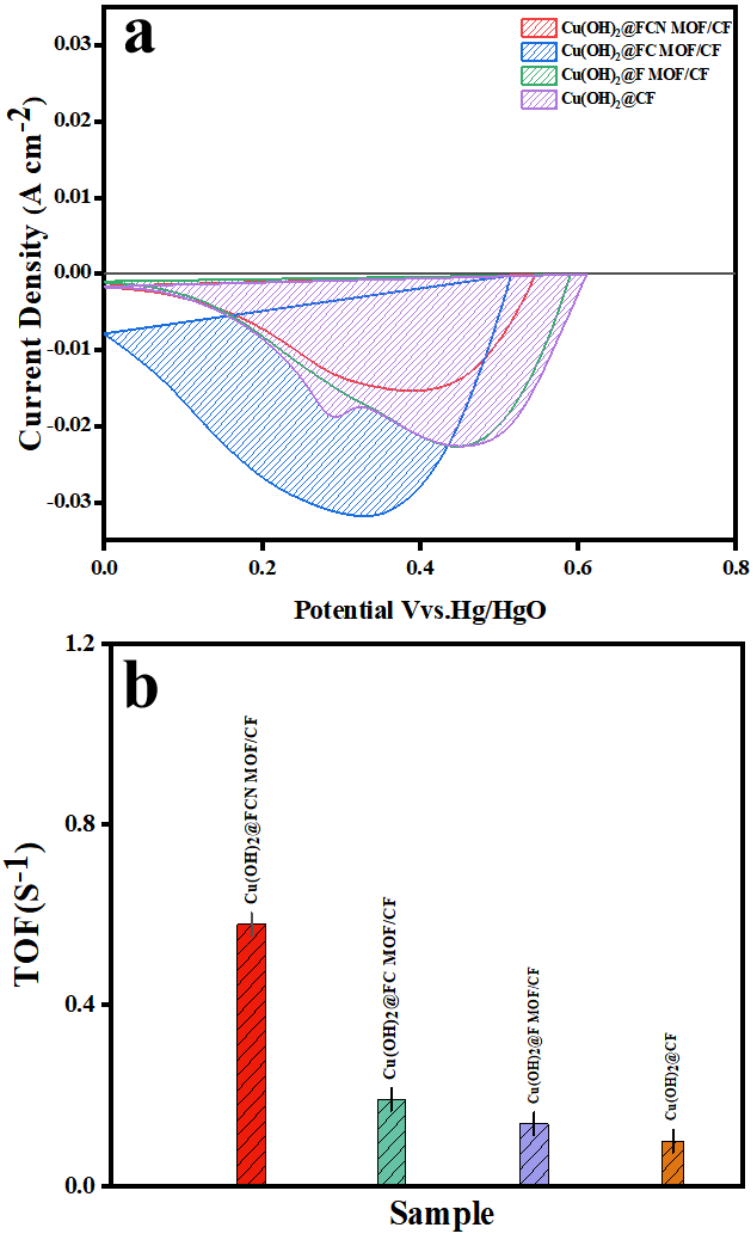

Figure S12. (a) Reduction peak acquired for the determination of surface active MOF species; (b)Turnover frequencies (TOF) of $Cu(OH)_2$@FCN MOF/CF, $Cu(OH)_2$@FC MOF/CF, $Cu(OH)_2$@F MOF/CF and $Cu(OH)_2$@CF.

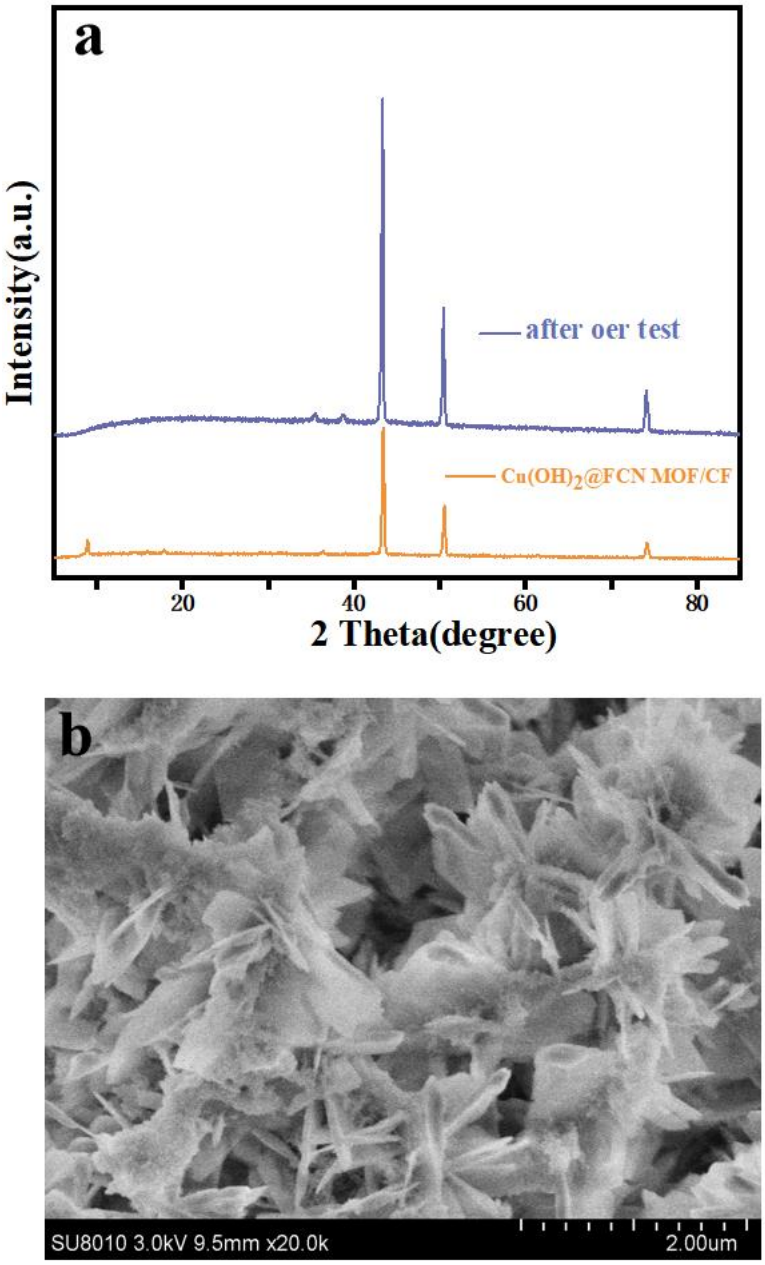

Figure S13. (a) Powder XRD patterns before and after OER test; (b) SEM image of $Cu(OH)_2$@FCN MOF/CF after OER test .

Table S1. Catalyst experimental error results.

Catalyst	Overpotential（10mA/cm²) vs.RHE）	C_{dl}(mF cm^{-2})	Tafel slope （mV·dec^{-1}）
$Cu(OH)_2$@FCN MOF/CF	242.00mV	315.06±0.017	96.15 ±0.267
$Cu(OH)_2$@FC MOF/CF	327.00mV	265.06±0.009	98.4±0.001
$Cu(OH)_2$@FMOF/CF	382.00mV	171.25±0.002	124.45±0.002
RuO_2@CF	348.00mV	201.9±0.001	100.71±0.00007
$Cu(OH)_2$@CF	421mV	78.24±0.001	158.79±0.004
CF	440mV	39.31±0.0009	231.57±0.002

Table S2. Performance Comparison of $Cu(OH)_2$@FCN MOF/CF catalysts and previously reported OER catalysts.

Catalyst	Electrolyte	Over Potential (10mA/cm²) vs.RHE	Tafel slope (mV dec^{-1})	Reference
d-PtSe	1 M KOH	310mV	129.3	**[47]**
Co_2P/CoP@NPGC	1 M KOH	340mV	116	**[48]**
Co-CeO_2/C	1 M KOH	380mV	99	**[49]**
Sm-$NiMnO_3$	1 M KOH	321mV	109	**[50]**
$NiFe_2O_4$ hollow fiber/Ni foam	1 M KOH	433mV	134	**[51]**
Ni_2P/Mn_2O_3	1M KOH	280mV	119.8	**[52]**
AC-$Co_2(OH)_3Cl$	1M KOH	272mV	151	**[53]**
CoP/NCNT/PC	1M KOH	282mV	103.7	**[54]**
Sc-CoBDC-3	1M KOH	300mV	125	**[55]**
$Cu(OH)_2$@FCNMOF/CF	1M KOH	255mV	**96.15**	**This work**

References:

47. Chang, Y.; Zhai, P.; Hou, J.; Zhao, J.; Gao, J. Excellent HER and OER Catalyzing Performance of Se-Vacancies in Defects-Engineered PtSe2: From Simulation to Experiment. Adv. Energy Mater. 2022, 12, 2102359.

48. Gong, W.; Zhang, H.; Yang, L.; Yang, Y.; Wang, J.; Liang, H. Core@shell MOFs derived Co2P/CoP@NPGC as a highly-active bifunctional electrocatalyst for ORR/OER. J. Ind. Eng. Chem. 2022, 106, 492-502.

49. Liu, Z.; Wan, J.; Li, M.; Shi, Z.; Liu, J.; Tang, Y. Synthesis of Co/CeO2 hetero-particles with abundant oxygen-vacancies supported by carbon aerogels for ORR and OER. Nanoscale 2022, 14, 1997-2003.

50. Silva, V. D.; Ferreira, L. S.; Simões, T. A.; Medeiros, E. S.; Macedo, D. A. 1D hollow MFe2O4 (M= Cu, Co, Ni) fibers by Solution Blow Spinning for oxygen evolution reaction. J. Colloid Interface Sci. 2019, 540, 59-65.

51. Swathi, S.; Yuvakkumar, R.; Ravi, G.; AlSehemibc, Abdullah G.; Velauthapillai, Dhayalan. Rare earth metal (Sm)-doped NiMnO3 nanostructures for highly competent alkaline oxygen evolution reaction. Nanscale adv. 2022, 4, 2235-2358.

52. Yang, B.; Chang, X.; Ding, X.; Ma, X.; Zhang, M. One-dimensional Ni2P/Mn2O3 nanostructures with enhanced oxygen evolution reaction activity. J. Colloid Interf. Sci. 2022, 625, 196-204.

53. Jiang, H.; He, Q.; Li, X.; Su, X.; Zhang, Y.; Chen, S.; Zhang, S.M.; Zhang, G.; Jiang, J.; Luo, Y.; Ajayan, P. M.; Song, L. Tracking Structural Self-Reconstruction and Identifying True Active Sites toward Cobalt Oxychloride Precatalyst of Oxygen Evolution Reaction. Adv. Mater. 2019, 31, 1805127.

54. Guo, Y.; Sun, Q.; Huang, Q.; Hu, Y.; Su, K.; Li, T. T.; Qian, J. Variable HOF-derived carbon-coated cobalt phosphide for electrocatalytic oxygen evolution. Carbon, 2022, 196, 457-465.

55. Huang, Q. Q.; Zhang, L. L.; Wu, P.; Zhang, M. C.; Liu, J. L.; Wu, J. S.; Ren, X. M. The morphology, crystal structure and oxygen evolution reaction electrocatalysis performance of scandium-doped MIL-101 (Fe). J. Solid State Chem. 2022, 312, 123202.